



## Article

# Remote Detection of Geothermal Alteration Using Airborne Light Detection and Ranging Return Intensity

Yan Restu Freski <sup>1,2,\*</sup> , Christoph Hecker <sup>1</sup> , Mark van der Meijde <sup>1</sup> and Agung Setianto <sup>2</sup>

<sup>1</sup> Faculty of Geo-Information Science and Earth Observation (ITC), University of Twente, Langezijds Building, Hallenweg 8, 7522 NH Enschede, The Netherlands

<sup>2</sup> Department of Geological Engineering, Faculty of Engineering, Universitas Gadjah Mada, Jl Grafika 2, Yogyakarta 55281, Indonesia

\* Correspondence: y.r.freski@utwente.nl or yan\_restu@ugm.ac.id

**Abstract:** The remote detection of hydrothermally altered grounds in geothermal exploration demands datasets capable of reliably detecting key outcrops with fine spatial resolution. While optical thermal or radar-based datasets have resolution limitations, airborne LiDAR offers point-based detection through its LiDAR return intensity (LRI) values, serving as a proxy for surface reflectivity. Despite this potential, few studies have explored LRI value variations in the context of hydrothermal alteration and their utility in distinguishing altered from unaltered rocks. Although the link between alteration degree and LRI values has been established under laboratory conditions, this relationship has yet to be demonstrated in airborne data. This study investigates the applicability of laboratory results to airborne LRI data for alteration detection. Utilising LRI data from an airborne LiDAR point cloud (wavelength 1064 nm, density 12 points per square metre) acquired over a prospective geothermal area in Bajawa, Indonesia, where rock sampling for a related laboratory study took place, we compare the airborne LRI values within each ground sampling area of a 3 m radius (due to hand-held GPS uncertainty) with laboratory LRI values of corresponding rock samples. Our findings reveal distinguishable differences between strongly altered and unaltered samples, with LRI discrepancies of approximately ~28 for airborne data and ~12 for laboratory data. Furthermore, the relative trends of airborne and laboratory-based LRI data concerning alteration degree exhibit striking similarity. These consistent results for alteration degree in laboratory and airborne data mark a significant step towards LRI-based alteration mapping from airborne platforms.

**Keywords:** hydrothermal alteration; geothermal surface manifestations; LiDAR return intensity



**Citation:** Freski, Y.R.; Hecker, C.; Meijde, M.v.d.; Setianto, A. Remote Detection of Geothermal Alteration Using Airborne Light Detection and Ranging Return Intensity. *Remote Sens.* **2024**, *16*, 1646. <https://doi.org/10.3390/rs16091646>

Academic Editors: Jorge Delgado García and Gianluca Groppelli

Received: 6 March 2024

Revised: 26 April 2024

Accepted: 1 May 2024

Published: 5 May 2024



**Copyright:** © 2024 by the authors. Licensee MDPI, Basel, Switzerland. This article is an open access article distributed under the terms and conditions of the Creative Commons Attribution (CC BY) license (<https://creativecommons.org/licenses/by/4.0/>).

## 1. Introduction

Remote detection and mapping for geothermal surface manifestation are critical for efficient exploration [1,2]. Remote techniques, therefore, have extensively been utilised for mapping surface manifestation to preliminarily assess geothermal systems beneath the surface (e.g., [3]). Hydrothermally altered ground, one target of remote mapping besides surface temperature anomalies, can give information towards the systems [4], as it indicates the hydrothermal process from its alteration degree. Thus, remote sensing techniques can be very valuable if they are able to detect and map alteration in geothermal systems.

Hydrothermal alteration on the surface can be regionally detected and remotely mapped due to the mappable size of their surface expressions, even from space. Many applications of spaceborne datasets (e.g., Advanced Spaceborne Thermal Emission and Reflection Radiometer (ASTER, spatial resolution 15 m), Hyperion (spatial resolution 30 m)) and airborne optical datasets (e.g., Airborne Visible/InfraRed Imaging Spectrometer (AVIRIS, spatial resolution 2.4 m) or AVIRIS-Next Generation (AVIRIS-NG, spatial resolution 8.1 m)) have been reported to map hydrothermal alteration effectively in large areas [3–11]. For smaller areas, employing unmanned aerial vehicles (UAVs) could be an

alternative to carrying remote sensors for mapping hydrothermal alteration, producing data in a higher spatial resolution, e.g., optical images of 0.05 m resolution [12]. However, the UAV platform can face limitations regarding power supply (i.e., battery life), making it challenging to use in early-stage exploration efforts over larger study areas.

Employing light detection and ranging (LiDAR, or laser scanning) is an alternative to optical, multi-, and hyper-spectral imaging to collect information on the ground surface in a finer spatial resolution. LiDAR acquisition typically produces data points in local XYZ coordinates, allowing an efficient and cost-effective way for a wide range of remote mapping applications [13]. This information about the coordinates with high point density is helpful to generate a high-resolution 3D model for surface expression (i.e., digital surface model, digital elevation model) and allow applications in more detail topographic mapping (e.g., landslides studies using a terrestrial laser scanner by [14]). Although the quality of LiDAR data depends on the point density, which is influenced by several factors of acquisition settings [15,16], LiDAR data can generate raster data with its finest ground sampling distance (GSD). For instance, the point density of 8 points/m<sup>2</sup> (e.g., in [17]) is equivalent to a GSD of  $\pm 0.3$  m.

Each data point is recorded with return intensity values (LiDAR return intensity, abbreviated as LRI in this study). LRI refers to the strength of the returning signal representing the target's reflectivity [18]. Sometimes, it is defined as the amount of energy received at the sensor [19]. As a discrete attribute of LiDAR, the LRI value depends on target reflectivity and other factors, such as incidence angle, target-sensor distance, and laser power [20]. Although various factors could influence LRI values, they represent the target (i.e., ground or rock) reflectivity at the laser wavelength. It can, therefore, potentially be used for hydrothermal alteration mapping when other airborne multi- and hyperspectral imagery (e.g., AVIRIS and AVIRIS-NG [5–8,10,11]) fails to map such small targets.

The potential uses of LRI values for rock discrimination have been reported from terrestrial laser scanners (TLS). Examples include discriminating marls from limestones [21], quartz-rich sandstones from clay-rich mudstones [22], limestones from cherts [23], various layers of marlstones, limestones, and interbedding mudstones [24], and marlstones and shales from limestones [25]. These studies demonstrated that rocks' typical characteristics (i.e., physical texture and chemical composition) are differentiable from their typical LRI responses. The expressions of rock layers on outcrops are also differentiable in LRI values (i.e., from a terrestrial scanner), which also allow further analyses of stratigraphic modelling [26] and geological structures (i.e., fold [24,25]). Although rock discrimination using LRI from terrestrial laser scanners (TLS) is well explored and opens up the possibility of using LRI values for mapping, LRI for mapping hydrothermal alteration from airborne platforms has received less attention.

The LRI response of hydrothermal rock alteration using TLS for LRI application to geothermal surface manifestation detection has previously been proven to be possible [27]. It demonstrated, at laboratory scale, that LRI values varied with alteration degree: strongly altered rocks showed much higher LRI values than unaltered rocks, with weakly altered rocks plotting between them. This relative order of LRI values for alteration stayed consistent with the alteration degree, even with different moisture levels. In this study, we show the possibilities for upscaling of the laboratory results to field level. We show that the relative variation in LRI, as observed in the laboratory, can also be found in the field. We explore the potential use of airborne LRI values for hydrothermal alteration detection by evaluating LRI values for different degrees of alteration as found in airborne LiDAR data. The airborne data, at the field sample locations, are validated with the laboratory results in the earlier study to confirm that patterns and trends in alteration degree and LRI do exist in airborne data, which potentially allows the use of LiDAR for future alteration mapping.

## 2. Materials and Methods

An airborne LiDAR dataset containing LRI values of hydrothermally altered outcrops was analysed to find the relationship between the order of alteration degree and the LRI

values. A series of rock samples were taken from the outcrops for a similar investigation in a laboratory environment [27]. Since the samples represent the outcrops, the laboratory results were used to confirm the observation of LRI trends in airborne data. The qualitative analysis was supported by correlation statistics. The details of the materials and methods are explained here.

### 2.1. Study Area

The airborne LRI data for the hydrothermally altered outcrops and non-altered areas was derived from an airborne LiDAR survey over the Bajawa Geothermal Field in the central part of Flores Island, Indonesia (Figure 1a,b). Bajawa was selected as the study area because the area has proven geothermal systems with the occurrence of hydrothermal alteration on the surface. The Indonesian State Electricity Company (PT PLN) has drilled production wells in Mataloko, a site with prominent heat anomalies within the Bajawa field [28]. Recent studies estimate that the Bajawa Geothermal Field has a total geothermal potential of 63 MW [29]. This potential resource is associated with active volcanism, as the field is located within the volcanic arc of the Lesser Sunda, with the field of monogenetic cones, and is surrounded by three active volcanoes, namely Mt. Inierie, Mt. Ebulobo, and Mt. Inielika [28].

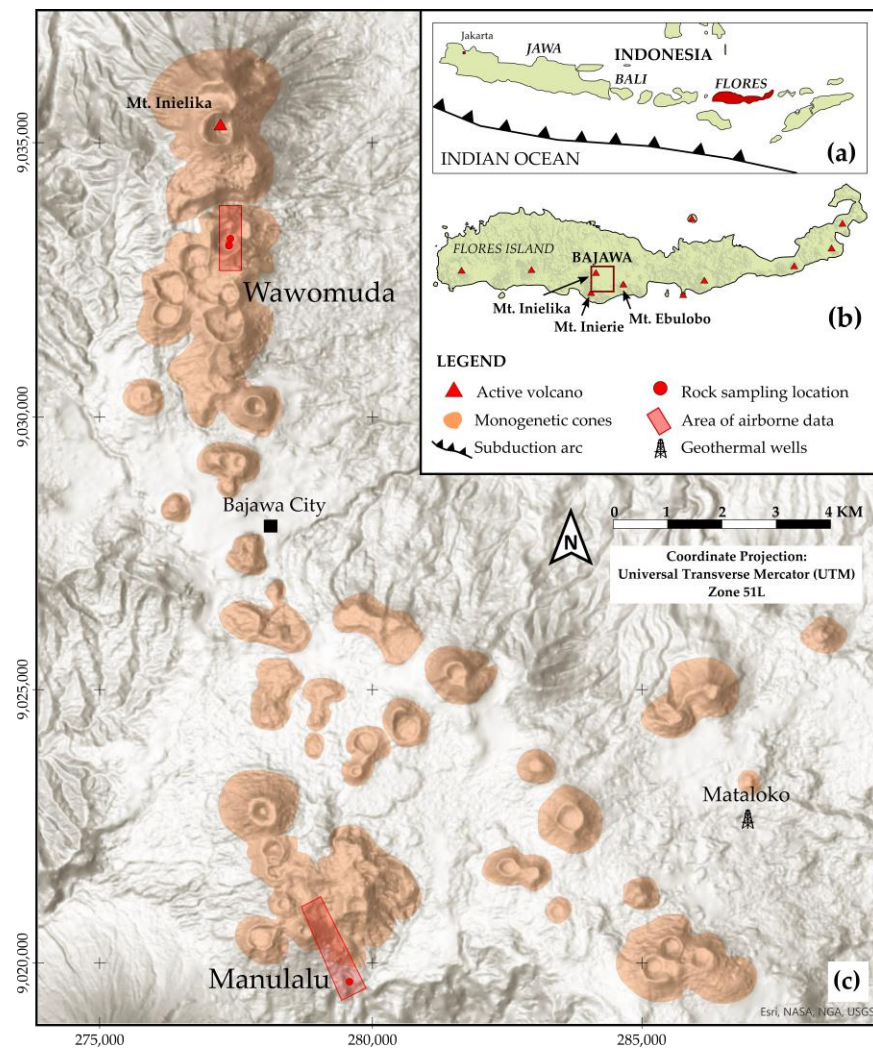


**Figure 1.** The study area is located in the Bajawa area, central Flores Island, Indonesia, and a part of the volcanic arc of the Lesser Sunda (a,b), surrounded by active volcanoes (Mt. Inierie, Mt. Inielika,

and Mt. Ebulobo in b) and monogenetic volcanoes (shaded with orange colour, (c)). The expressions of the volcanic activity on the surface indicate the presence of geothermal systems beneath the Bajawa City and Mataloko production well (c). The airborne datasets were obtained from Wawomuda and Manulalu (shaded with red in (c)) and covered the sampling locations (red dots with sample names in (c)). The hill-shaded topographic map on the background (including the modified inset map) is available from ESRI.

The specific locations for this study are Wawomuda and Manulalu (Figure 1c), where the airborne dataset covers representative areas for all alteration degrees. Wawomuda is a prominent crater of Mt. Inielika complex that had its latest phreatic-type eruption in early 2001 (see Mt. Inielika's record by [30]), exposing the hydrothermally altered ground in the crater (Figure 2a,c). Meanwhile, unaltered conditions are found in Manulalu, where a breccia of unaltered volcanic rocks is exposed at the surface (Figure 2b,d).

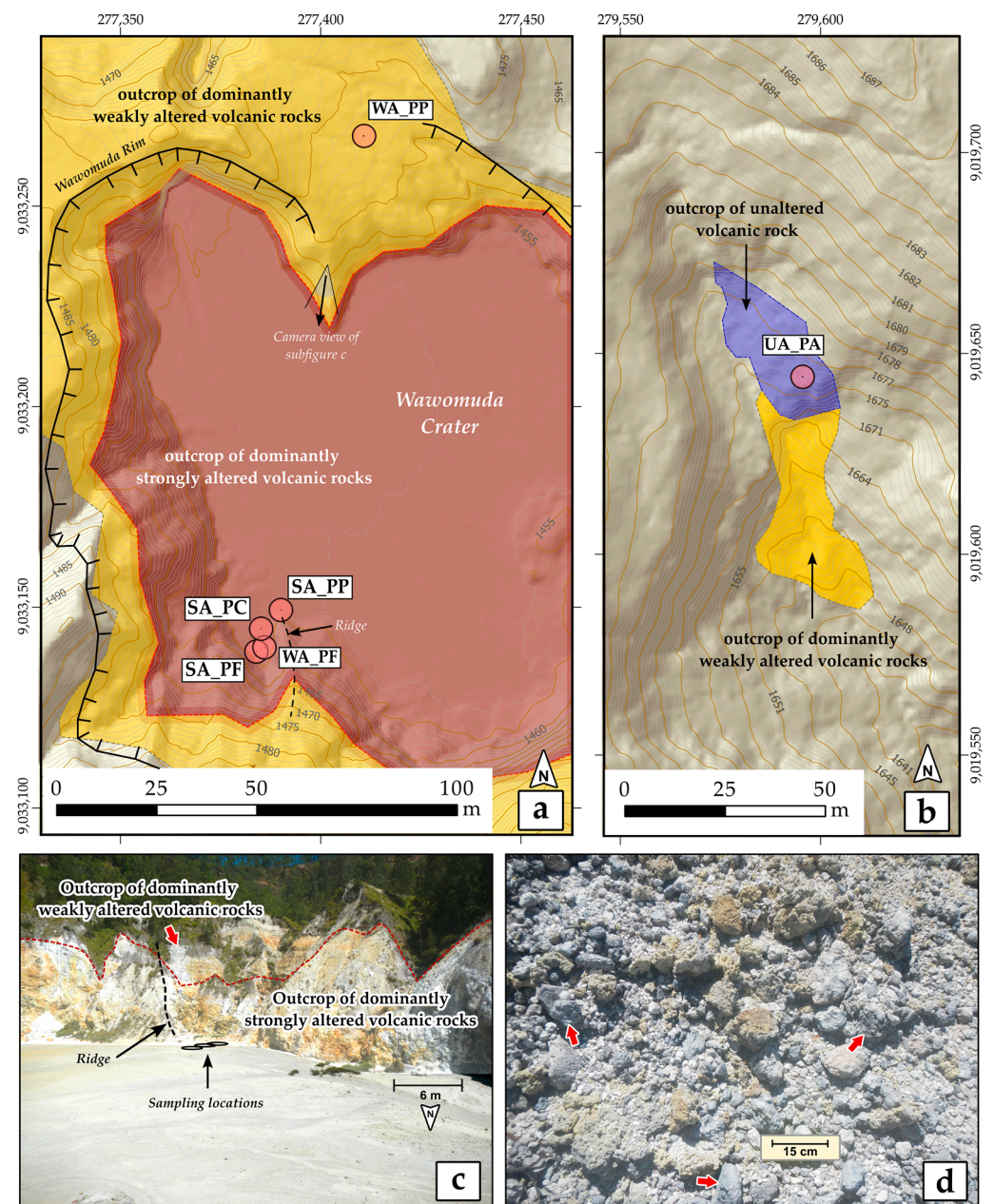


**Figure 2.** Field alteration map and photographs showing the outcrops and the sampling location in Wawomuda (a,c) and Manulalu (b,d). In Wawomuda, the samples were collected at the foot of

the crater wall (a,c). The outcrop of strongly altered rocks (i.e., the source of SA\_PC, SA\_PP, and SA\_PF) builds up the lower section of the Wawomuda Crater wall with weakly altered rocks above it (i.e., the source of WA\_PF) with no solid boundary (red dashed line). The sampling location of WA\_PP is behind the observer (c). In Manulalu, the outcrop is composed of a breccia of unaltered volcanic rock (i.e., the source of UA\_PA; see the breccia fragments pointed by red arrows in (d)). The hill-shaded topographic map on the background is generated from the LiDAR dataset.

## 2.2. Sampling Locations and Rock Samples

Six (6) sampling locations were carefully selected, considering the representation across all alteration degrees, including strongly altered, weakly altered, and unaltered rocks. These locations were chosen as the sites for collecting hand-sized rock samples intended for laboratory analysis, and for comparison between field and airborne data (see the sampling location in Figure 1 and Table 1). Although the sample locations are more than 10 km apart, all samples were from the same host rock (i.e., basaltic-andesitic volcanic rock [28]). The samples were ranked according to alteration degree based on the remaining rock texture observed by hydrothermal alteration experts as a product of the alteration process.

**Table 1.** A list of geothermal rock samples analysed for LRI under laboratory conditions (after [27]). These rocks are ordered and grouped based on the degree of alteration defined by their physical expression. All altered rocks were sampled in Wawomuda, while the unaltered sample was collected in Manulalu.

Alteration Degree	Description	Photograph	Sample Code	Sampling Coordinates in UTM (Zone 51L)
	Strongly altered porous fine-grained lapilli-tuff		SA_PF	277383 9033139
	Strongly altered porous porphyritic autobreccia		SA_PP	277389 9033149
	Strongly altered porous coarse-grained breccia		SA_PC	277384 9033145
	Weakly altered porous fine-grained lapilli-tuff		WA_PF	277385 9033140
	Weakly altered porous porphyritic andesite		WA_PP	277411 9033267
	Unaltered porous aphanitic scoriaceous basalt		UA_PA	279596 9019644

### 2.3. Airborne LiDAR Datasets

The airborne LRI values were acquired using a Leica ALS70 scanner (at 1064 nm) aboard a Pilatus Porter PC-6 aircraft modified for LiDAR surveys. Flying at a nominal height of 800 m minimised cloud cover issues typical in tropical areas, ensuring optimal LiDAR reflection. The scanner, operating at a ground velocity of 213 km/h, yielded datasets with an average point density of 12 points/m<sup>2</sup>, higher at flight line edges due to data overlap. At an altitude of 800 m, the laser footprint was approximately 10 cm in diameter, comparable to laboratory sample sizes. The scanning swath, with a field of view of 22°, reached a width of around 270 m on the ground. Geodetic GPS receiver and inertia measurement unit (IMU) onboard ensured spatial accuracy, reported at 0.76 cm [31].

The airborne surveys were conducted during the early dry season (late May to early June 2018) when significant rainfalls of the rainy season had already ceased (for rainfall data, see nearby station [32]). Consequently, the survey successfully avoided high soil moisture conditions for such a tropical area in Indonesia, which could potentially affect the LRI values [27].

This study utilises processed LRI values at ‘Level 1’, which have undergone geometric corrections [33]. The data provider conducted these corrections as part of their standard processing chain for the Leica ALS70 data. Since the study focuses on understanding relative trends in LRI values rather than analysing data for classification based on absolute values, further processing steps, such as atmospheric corrections, were omitted. The data level is sufficient for this study with the relative trends in the data remain unaffected by external factors.

The input LiDAR point clouds comprised multiple returns from each laser pulse, reflecting off the ground or various vegetation layers above. To simplify this initial study, and given that hydrothermal alteration outcrops typically lack vegetation, the airborne LRI investigation focused on vegetation-free, bare-ground areas coinciding with laboratory sample collection sites. Thus, only bare-ground LiDAR reflections were considered. To ensure this, two standard measures were taken. Firstly, non-ground points were filtered out using a Cloth Simulation Filter (CSF, [34]) in CloudCompare, eliminating points originating from vegetation. The CSF mechanism inverts the LiDAR data points and simulates a cloth surface covering the inverted data points. This filter calculates a new position for data points at any void between the surrounding data points. The CSF is derived from Newton’s second law, which considers only gravity force when calculating the displacement of data points. Such modification to the formula allows simple calculation for the current position of a data point (1) if the initial position ( $X$ ) and the time step ( $\Delta t$ ) is known (mass ( $m$ ) is set 1, and  $G$  is gravity constant [34]):

$$X(t + \Delta t) = 2X(t) - X(t - \Delta t) + \frac{G}{m} \Delta t^2 \quad (1)$$

The CSF, optimised for relief terrain data, employed a cloth resolution of 0.1 m to retain dataset details, although it might struggle with steep volcanic terrain. Secondly, only ground return points reflecting solely from the ground surface, without energy reflected off the canopy, were selected. Points with additional canopy reflections were excluded, ensuring the optimum LRI values. The LRI values of valid ground points around the sampling location were then averaged within a 3 m radius (acknowledging GPS accuracy).

### 2.4. Validation of LRI for Hydrothermal Alteration

All LRI values, both laboratory and airborne, were processed and normalised (scale 0–100) to allow for comparison between experiments. Note that the validation and normalisation aimed for LRI values at their relative values between alteration stages since the study explores the pattern of LRI values in airborne LiDAR data. This therefore implies that we aim with this research for a qualitative comparison (separation of value (ranges) between alteration stages).

According to the earlier laboratory study, increasing LRI values linearly correlate with increasing alteration degree. A trend analysis was carried out to highlight whether a distinct linear relationship was visible. The evaluation also considers the standard deviation for each sample to see if a group of altered rocks is distinguishable in LRI values from the fresh rock. A statistical analysis, i.e., Pearson’s correlation coefficient, was calculated to examine the relationship between the datasets.

### 3. Results

The comparison between airborne LRI values within a 3 m radius of sampling locations and laboratory LRI values reveals two key findings: similarity in increasing trends with alteration degree and separability of each degree in both LiDAR systems. A statistical summary is presented in Table 2 and visually depicted in Figure 3.

**Table 2.** A statistical summary of LRI values for each sample in the laboratory (using terrestrial laser scanning, TLS) and airborne (using airborne laser scanning, ALS). Note that the airborne LRI values are lower than those from the laboratory.

Measures	UA_PA		WA_PP		WA_PF		SA_PC		SA_PP		SA_PF	
	TLS	ALS										
Mean	71.69	25.65	78.86	37.80	83.53	56.03	82.59	52.70	86.16	59.22	84.79	49.69
Median	71.08	26.00	79.04	38.00	83.88	56.00	82.76	52.00	86.27	59.00	85.39	52.00
Standard deviation	3.29	6.43	1.69	4.85	1.64	8.49	1.60	7.16	1.07	7.62	1.55	13.65
Minimum	64.48	10.00	72.74	23.00	76.06	22.00	75.43	34.00	80.70	29.00	78.65	12.00
Maximum	81.86	86.00	84.03	58.00	86.76	92.00	87.45	79.00	89.11	79.00	87.10	92.00
Interquartile range	4.93	8.25	2.20	7.00	1.61	11.00	2.20	9.50	1.27	9.00	1.61	15.00

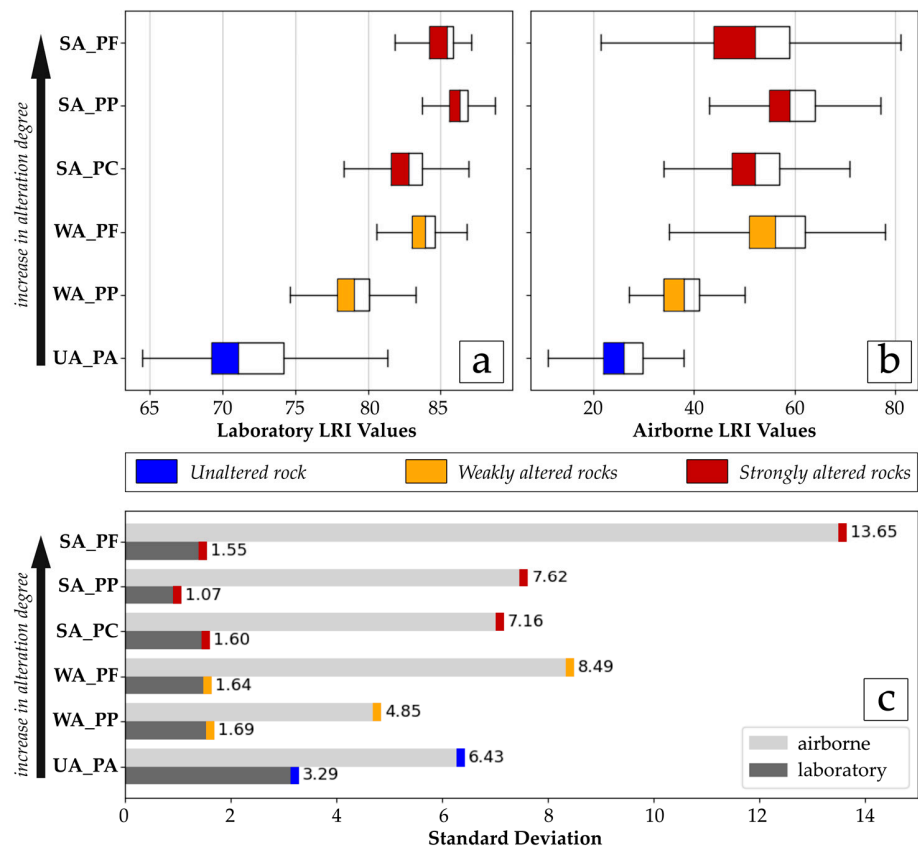


**Figure 3.** The comparison of LRI trends from the laboratory ((a), from [27]) and the airborne dataset (b). The increasing trends similarly show that higher LRI values result from higher alteration degrees (a,b). The standard deviations of the LRI values from the airborne data are larger than those derived from samples in the laboratory (c).

The first finding reveals a strikingly similar trend in relative LRI values across alteration degrees in both datasets (Figure 3a,b and Figure 4). In the airborne dataset, LRI values consistently increase with alteration degrees from unaltered to strongly altered ground. The trend analysis shows that the airborne data are comparable with the laboratory data in a linear way with an R-square of 0.92 (Figure 4). This is supported by a strong positive linear relationship, with a Pearson's correlation coefficient of 0.95. The  $p$ -value for Pearson's coefficients is 0.002, indicating statistical significance at the 0.05 level. It is evident from the observations that although the trends are very similar, the absolute values differ, with lower airborne LRI values at all sampling locations.

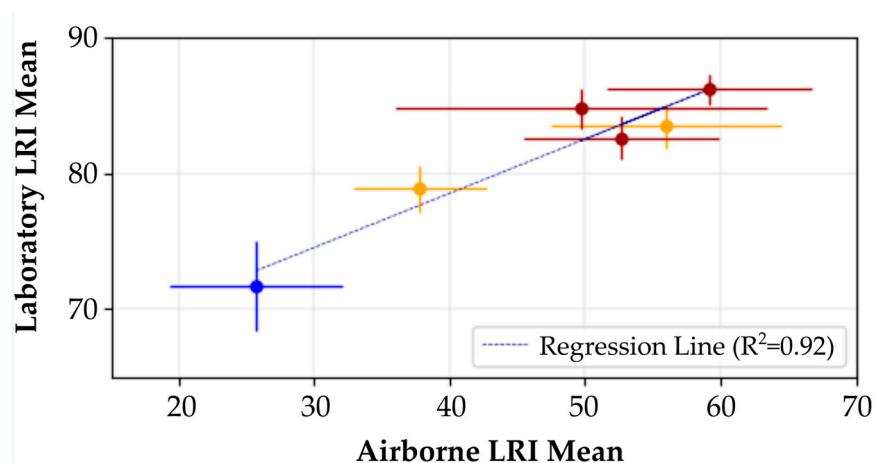


**Figure 4.** The linear relationship between airborne and laboratory LRI mean (the colour refers to Figure 3). The regression line with an  $R^2$  of 0.92 means that both airborne and laboratory data share a strong linear relationship. LRI values increase in both datasets with alteration degree (with the exception of one sample of weakly altered rocks plotting between the strongly altered samples). Note that both LRI datasets have been normalised at the comparable range.

The second similarity is evident in the distinction between strongly altered and fresh rocks/outcrops in the sampling area. Airborne LRI values of strongly altered grounds (e.g., SA\_PP, SA\_PC, SA\_PF) cluster at the highest values, approximately 45–63 (see sample boxes in Figure 3b). Conversely, airborne LRI values of unaltered ground (e.g., UA\_PA) are notably lower ( $LRI < 30$ ), with weakly altered ground (e.g., WA\_PP) exhibiting intermediate values between strongly altered and unaltered ground. Notably, one weakly altered sample, WA\_PF, displays LRI values similar to strongly altered samples despite its classification based on physical appearance. It is, however, clear that this sampling location is very close to SA\_PF, and in the LiDAR data, for a large part overlapping in area with SA\_PF. The similarity between SA\_PF and WA\_PF can, therefore, be explained by the sampling at very near locations.

The similarities are noteworthy as they arise from two different LiDAR scanning systems. Differences in scanning systems are reflected in absolute LRI values between laboratory and airborne data. Laboratory LRI values, obtained under controlled conditions, are higher and exhibit tighter variability (i.e., low standard deviation) than airborne LRI values. Standard deviation values for airborne LRI are up to nine times larger than in laboratory data, with trends showing opposite directions. In airborne data, the standard deviation of LRI values increases with alteration degree, while it remains stable in laboratory data (Figure 3c).

On the map, LRI values within the 3 m sampling area surrounding UA\_PA and WA\_PP exhibit a relatively uniform distribution (with an average of 25.65 and an interquartile range of 8.25 for UA-PA, and an average of 37.8 with an interquartile range of 7 for WA\_PP; depicted green in Figure 5a and yellow in Figure 5c, respectively). Conversely, strongly altered grounds in Wawomuda exhibit more variable LRI values, mostly red with some

yellow (Figure 5e), compared to unaltered and weakly altered areas (Figure 5a,c). Despite its weakly altered classification, WA\_PF ground is a bit outside the trend, displaying high LRI values. These observations, along with terrain analysis (Figure 5b,d,f), will be further discussed in Section 4 Discussion.

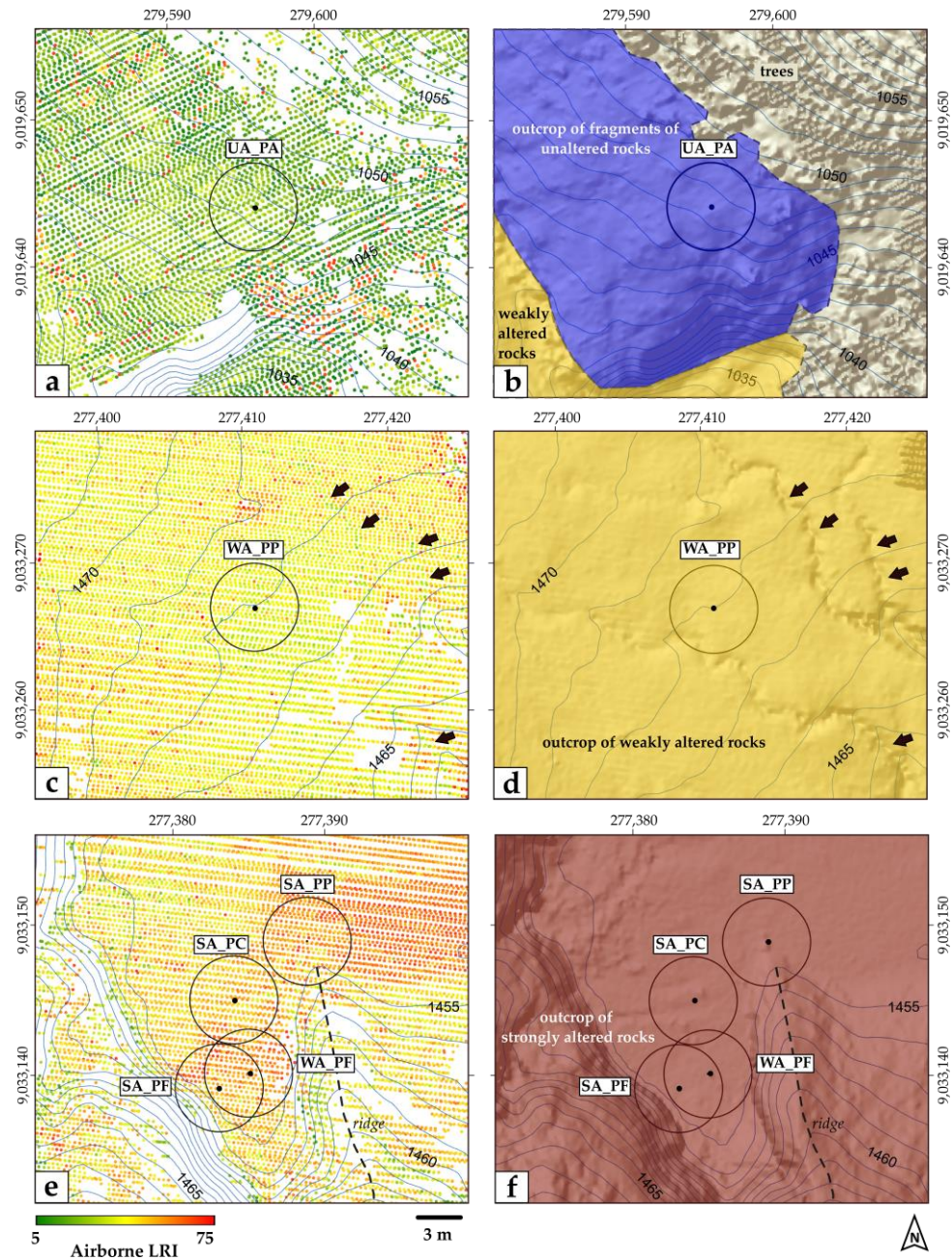


**Figure 5.** Sampling areas with filtered and coloured airborne LRI points (a,c,e) and corresponding alteration degree from field work (b,d,f), respectively. Note that points with low LRI are found along gullies (see all arrows in (c,d)). For clarity in orientation with the outcrop photograph (Figure 2a), the ridge next to the sampling locations is indicated with an orange dashed line (f). The hill-shaded topographic map with contour lines in metres in the background is generated from the LiDAR point cloud.

#### 4. Discussion

Our results show that the trends of LRI values found in the laboratory are similar to those in the airborne data for the sampling locations of the laboratory samples. LRI values increase with alteration degrees from unaltered- and weakly altered- to strongly altered

ground (Figure 3a,b), although there are differences in detail due to two different scanning systems (e.g., standard deviation values, Figure 3c). In airborne data, the distribution of LRI values of unaltered and weakly altered ground is more uniform than the LRI values of strongly altered ground, which are spatially more variable (Figure 3a,c,e). Here, we discuss our findings and the possibility of the application of airborne LRI for hydrothermal alteration mapping.

#### 4.1. Comparison with Laboratory Results

For both airborne and laboratory LRI data, we observe that the higher LRI values are shown for the stronger alteration degrees. At the wavelengths of both LiDAR scanners, targets with strong alteration reflect the most energy of the scanner's laser beam of all the samples. The difference in return intensity between the two platforms is likely related to the increased complexity of airborne acquisition, e.g., atmospheric absorption [17,20,33–38]. Since our laboratory data are collected from a short distance and perpendicular to the general sample surface, this represents the target reflectivity [27]. Our airborne data are corrected for range and incidence angle [31]; hence, our datasets are comparable in a relative sense. No atmospheric correction is performed on either of them since there are various ways to do this (as summarised by [33]), and each will lead to slightly different intensity values. The same may also happen when our method is applied to other datasets. Therefore, we aim to define relative separation within intensity data to separate the different alteration levels rather than doing this in an absolute sense. While our two datasets show a shift between them in the absolute sense, the different populations are separable in a relative sense within each dataset (Figure 3a,b).

Moreover, this complexity in the airborne data only causes lower LRI values and broader standard deviations. Despite the lower LRI values, the separability of each alteration degree in airborne is still present and even more pronounced than in the laboratory data (Figure 3a,b). Our results also show that the LRI values' standard deviation increases with the airborne data's alteration degree. At the same time, it appears to be less dependent on the alteration degree for the laboratory data (Figure 3c). We attribute this higher standard deviation of the airborne LRI values to other influencing ground conditions within each sampling location, which will be discussed in 4.2. Variability in Airborne LRI Values, Limitations, and Challenges.

One sample that does not strictly follow the LRI–alteration degree relationship is WA\_PF. This sample consistently (in the laboratory and airborne LRI results) plots more amongst the strongly altered samples than the weakly altered ones. Since the alteration degree was determined by visual inspection based on the physical description (see [27]) and since no additional analytics are available for this dataset, we assume that this sample's original alteration degree may have been judged to be lower than it is.

#### 4.2. Variability in Airborne LRI Values, Limitations, and Challenges

The statistics of each sampling location are calculated within the 3 m radius. This radius is a consequence of the ability of the hand-held GPS Garmin 62 to pinpoint the sampling location. Therefore, the homogeneity of the outcrop will be seen in the standard deviation, where a more significant standard deviation means that the outcrop is less homogeneous. The outcrop can be variable within the sampling area regarding alteration degree (as it is the target to be mapped), outcrop geomorphology, and soil moisture.

##### 4.2.1. Variability Due to Alteration Degree

The interpretation of the results is based on the limited number of samples from a homogeneous host rock, basaltic-andesitic volcanic rock [28]. This series of rocks differ in colour from dark (i.e., unaltered rock) to bright (i.e., strongly altered rock). The rock colour is the manifestation of mineral content [39]. Thus, the mineral content seems to influence the airborne LRI values, as it also influences the laboratory LRI values [27]. Since our host lithology is naturally dark, and the alteration products are more reflecting, increasing the

alteration degree will lead to brighter samples (in the visible, but evidently also in the near-infrared wavelengths the LRI is measured in). This relationship may not be applicable to all other host lithologies. One example that should be tested is a rhyolitic environment where the original, unaltered host rock is substantially brighter than the mafic volcanic rocks tested here.

The effect of colour variation on rock surface due to weathering process (i.e., not hydrothermal alteration) that may contribute to decreased LRI values in laboratory (as in [27]) is difficult to see in the airborne data. This is because the LRI values of each sample need to be calculated from a 3 m radius of each sampling location, while the weathering effect of the ground will never occur uniformly for that circle size. For instance, the sample SA\_PF that shows a weathering surface and is considered insignificant to change the trend of LRI values in the laboratory [27] does not necessarily cause the decrease in the LRI values in the airborne data (see SA\_PF in Figure 3b). The drop in the averaged LRI values is because of the low LRI values on the cliff, i.e., suggesting it has a low alteration degree (Figures 2a, 4f and 5e).

#### 4.2.2. Variability Due to Outcrop Geomorphology

The data of the cliff in the vicinity of the sampling area are excluded from the results (i.e., shown as no data in the LRI map, Figure 5), while the alteration on the cliff wall may be a key outcrop (i.e., for its weakly altered degree). The chosen filter CSF removes the data because the relative distribution of the data points resembles the vertical structure of trees, while the filter works based on the horizontality of the point cloud's structures [34]. The filter distinguishes the multiple points of objects (i.e., trees, if any) that are not desired in the ground detection. The filter is selected in this study because it works satisfyingly for the sampling locations in an open and mostly flat area. Thus, alteration mapping in a larger area requires a filter applicable to various settings by the changes in the outcrop geomorphology to keep the ground data intact for interpretation.

Terrestrial scanners can also be an alternative for completing the void in the filtered airborne data. Such detailed remote mapping of a vertical outcrop using terrestrial scanners has been extensively demonstrated (e.g., [23–26,40]). Since the resulting LRI values from a terrestrial platform have been tested for hydrothermal alteration in the earlier work [27] and those from airborne in this study, LRI values from both terrestrial and airborne could be directly combined.

#### 4.2.3. Variability Due to Soil Moisture

Soil moisture has been reported to decrease LRI values [22,41,42], although homogeneous soil moisture content would still leave the relative LRI values intact [27]. However, the effect of soil moisture in the sampling location of the study (i.e., within the 3 m radius) has less impact on the LRI values. There was no precipitation during the airborne LiDAR scanning campaign, and no steaming activity in the area (Figure 2), and the soil moisture effect is assumed to be minimal. Only at a small part of the adjacent ground of the sampling location are there shallow gullies where the water can accumulate and tends to be wetter than the other higher ground (see the small traces of gullies with lower LRI values in Figure 5c,d). If the acquisition campaign is held in the wet season, it may not be a good time to map the ground as the LRI values of the ground will significantly drop from the original value.

#### 4.3. Outlook for Airborne Applications

The results of this study present a qualitative link between LRI values and alteration degree, which is consistent between the two acquisition modes (i.e., laboratory and airborne) for the samples, and their corresponding locations, in the study area. In order to apply the results to airborne alteration mapping over a larger area with more complex ground conditions, higher processing levels of LRI values (e.g., correction for atmospheric effect when needed) may be required to allow comparisons between different areas. Additional

information from other datasets with comparable resolution (e.g., for soil moisture) will provide further insight into the impact of additional environmental conditions on the observed LRI values. Vegetation can impact the results in two ways. Firstly, short vegetation at ground level, like grass, could pose a potential problem as it cannot be separated from the outcrop target using the ground filter used in this study. Additional data layers, like vegetation indexes, could detect possible issues. Secondly, in areas with high vegetation, mapping the ground below the vegetation canopy requires modelling energy loss due to multiple returns of a single LiDAR beam. If part of the energy is reflected off layers inside the canopy, only a fraction of the beam intensity is available at the ground level to be reflected. Applying multi-targets and multiple scattering models may help translate these early results of using LRI into a workable tool for alteration mapping below the canopy. A more extensive statistical analysis for future research will allow further insight into the complex relationship between data sources and geothermal phenomena.

## 5. Conclusions

The results of this study demonstrate the relation between LRI values in the laboratory [27] and airborne LiDAR data (this study) for a range of hydrothermal alterations in rocks: the higher the alteration degree, the higher the LRI values. This is evident in the trend analysis of LRI values from the lab vs. airborne data and the separability of altered rocks from unaltered ones. With laboratory tests on the limited number of samples as a basis and a consistent order of alteration degree in airborne data for the sampling locations, this study opens up the potential use of airborne LRI values for detecting hydrothermally altered ground in local or regional areas. We have found a consistent qualitative trend in LRI values from unaltered to strongly altered ground, which can form the basis for airborne alteration mapping in more complex situations. Future research should investigate how the quantitative modelling of multiple canopy returns and additional ground information, such as soil moisture, can impact the mapping of alteration and the extent to which more detailed information is required on these parameters to be able to use LRI as a mapping tool for hydrothermally altered areas.

**Author Contributions:** Conceptualization, Y.R.F.; methodology, Y.R.F. and C.H.; software, Y.R.F.; validation, C.H., M.v.d.M. and A.S.; formal analysis, Y.R.F.; investigation, Y.R.F.; resources, Y.R.F.; data curation, Y.R.F. and C.H.; writing—original draft preparation, Y.R.F.; writing—review and editing, C.H. and M.v.d.M.; visualisation, Y.R.F.; supervision, C.H., M.v.d.M. and A.S.; project administration, Y.R.F.; funding acquisition, C.H. and M.v.d.M. All authors have read and agreed to the published version of the manuscript.

**Funding:** This research was funded by the Dutch Ministry of Foreign Affairs through the Geothermal Capacity Building Program Indonesia–Netherlands (GEOCAP), number 2000 0478-10. PT. ASI Pudjiastuti Geosurvey conducted and co-financed the airborne LiDAR acquisition part of the project.

**Data Availability Statement:** The data presented in this study are available on request from the corresponding author due to legal reasons.

**Acknowledgments:** We would like to thank Robert Hewson and the anonymous reviewers for their constructive suggestions, which greatly improved this article. We also thank Sander Oude Elberink (ITC) and Harintaka (UGM) for the discussion about LiDAR.

**Conflicts of Interest:** The authors declare no conflicts of interest. The funders had no role in the design of the study; in the collection, analyses, or interpretation of data; in the writing of the manuscript; or in the decision to publish the results.

## References

1. van der Meer, F.; Hecker, C.; van Ruitenbeek, F.; van der Werff, H.; de Wijkerslooth, C.; Wechsler, C. Geologic Remote Sensing for Geothermal Exploration: A Review. *Int. J. Appl. Earth Obs. Geoinf.* **2014**, *33*, 255–269. [[CrossRef](#)]
2. Yalcin, M.; Kilic Gul, F.; Yildiz, A.; Polat, N.; Basaran, C. The Mapping of Hydrothermal Alteration Related to the Geothermal Activities with Remote Sensing at Akarcay Basin (Afyonkarahisar), Using Aster Data. *Arab. J. Geosci.* **2020**, *13*, 1166. [[CrossRef](#)]

3. Calvin, W.M.; Littlefield, E.F.; Kratt, C. Remote Sensing of Geothermal-Related Minerals for Resource Exploration in Nevada. *Geothermics* **2015**, *53*, 517–526. [[CrossRef](#)]
4. Abubakar, A.J.; Hashim, M.; Pour, A.B. Identification of Hydrothermal Alteration Minerals Associated with Geothermal System Using ASTER and Hyperion Satellite Data: A Case Study from Yankari Park, NE Nigeria. *Geocarto. Int.* **2019**, *34*, 597–625. [[CrossRef](#)]
5. Hellman, M.J.; Ramsey, M.S. Analysis of Hot Springs and Associated Deposits in Yellowstone National Park Using ASTER and AVIRIS Remote Sensing. *J. Volcanol. Geotherm. Res.* **2004**, *135*, 195–219. [[CrossRef](#)]
6. Kruse, F.A. Comparative Analysis of Airborne Visible/Infrared Imaging Spectrometer (AVIRIS), and Hyperspectral Thermal Emission Spectrometer (HyTES) Longwave Infrared (LWIR) Hyperspectral Data for Geologic Mapping. In *Proceedings of the SPIE 9472, Algorithms and Technologies for Multispectral, Hyperspectral, and Ultraspectral Imagery XXI, Baltimore, MD, USA, 20–24 April 2015*; Velez-Reyes, M., Kruse, F.A., Eds.; SPIE: Bellingham, WA, USA, 2015; Volume 9472.
7. Kumar, H.; Ramakrishnan, D.; Jain, R.; Govil, H. Can Imaging Spectroscopy Divulge the Process Mechanism of Mineralization? Inferences from the Talc Mineralization, Jahazpur, India. *Remote Sens.* **2023**, *15*, 2394. [[CrossRef](#)]
8. Mishra, G.; Govil, H.; Srivastava, P.K. Identification of Malachite and Alteration Minerals Using Airborne AVIRIS-NG Hyperspectral Data. *Quat. Sci. Adv.* **2021**, *4*, 100036. [[CrossRef](#)]
9. Pour, A.B.; Hashim, M.; van Genderen, J. Detection of Hydrothermal Alteration Zones in a Tropical Region Using Satellite Remote Sensing Data: Bau Goldfield, Sarawak, Malaysia. *Ore. Geol. Rev.* **2013**, *54*, 181–196. [[CrossRef](#)]
10. Roy, S.; Bhattacharya, S.; Omkar, S.N. Automated Large-Scale Mapping of the Jahazpur Mineralised Belt by a MapReduce Model with an Integrated ELM Method. *PFG—J. Photogramm. Remote Sens. Geoinf. Sci.* **2022**, *90*, 191–209. [[CrossRef](#)]
11. Tripathi, M.K.; Govil, H.; Bhaumik, P. Implications and Interrelations of Litho-Boundaries and Vicinity of Lineaments for Hydrothermal Alteration Zones under Remote Sensing and GIS Environment. *Adv. Space Res.* **2022**, *70*, 621–640. [[CrossRef](#)]
12. Müller, D.; Bredemeyer, S.; Zorn, E.; De Paolo, E.; Walter, T.R. Surveying Fumarole Sites and Hydrothermal Alteration by Unoccupied Aircraft Systems (UAS) at the La Fossa Cone, Vulcano Island (Italy). *J. Volcanol. Geotherm. Res.* **2021**, *413*, 107208. [[CrossRef](#)]
13. Beraldin, J.-A.; Blais, F.; Lohr, U. Airborne and Terrestrial Laser Scanning. In *Airborne and Terrestrial Laser Scanning*; Vosselman, G., Maas, H.-G., Eds.; Whittles Publishing: Scotland, UK, 2010; pp. 1–44, ISBN 9781904445876.
14. Jaboyedoff, M.; Oppikofer, T.; Abellán, A.; Derron, M.-H.; Loye, A.; Metzger, R.; Pedrazzini, A. Use of LIDAR in Landslide Investigations: A Review. *Nat. Hazards* **2012**, *61*, 5–28. [[CrossRef](#)]
15. Jia, Y.; Lan, T.; Peng, T.; Wu, H.; Li, C.; Ni, G. Effects of Point Density on DEM Accuracy of Airborne LiDAR. In *Proceedings of the 2013 IEEE International Geoscience and Remote Sensing Symposium—IGARSS, Melbourne, Australia, 21–26 July 2013*; pp. 493–496. [[CrossRef](#)]
16. Petras, V.; Petrasova, A.; McCarter, J.B.; Mitasova, H.; Meentemeyer, R.K. Point Density Variations in Airborne Lidar Point Clouds. *Sensors* **2023**, *23*, 1593. [[CrossRef](#)]
17. Wu, Q.; Zhong, R.; Dong, P.; Mo, Y.; Jin, Y. Airborne LiDAR Intensity Correction Based on a New Method for Incidence Angle Correction for Improving Land-Cover Classification. *Remote Sens.* **2021**, *13*, 511. [[CrossRef](#)]
18. Jelalian, A.V. *Laser Radar Systems*; Artech House: Boston, MA, USA, 1992; ISBN 9780890065549, 0890065543.
19. García, M.; Riaño, D.; Chuvieco, E.; Danson, F.M. Estimating Biomass Carbon Stocks for a Mediterranean Forest in Central Spain Using LiDAR Height and Intensity Data. *Remote Sens. Environ.* **2010**, *114*, 816–830. [[CrossRef](#)]
20. Coren, F.; Sterzai, P. Radiometric Correction in Laser Scanning. *Int. J. Remote Sens.* **2006**, *27*, 3097–3104. [[CrossRef](#)]
21. Franceschi, M.; Teza, G.; Preto, N.; Pesci, A.; Galgaro, A.; Girardi, S. Discrimination between Marls and Limestones Using Intensity Data from Terrestrial Laser Scanner. *ISPRS J. Photogramm. Remote Sens.* **2009**, *64*, 522–528. [[CrossRef](#)]
22. Burton, D.; Dunlap, D.B.; Wood, L.J.; Flaig, P.P. Lidar Intensity as a Remote Sensor of Rock Properties. *J. Sediment. Res.* **2011**, *81*, 339–347. [[CrossRef](#)]
23. Penasa, L.; Franceschi, M.; Preto, N.; Teza, G.; Polito, V. Integration of Intensity Textures and Local Geometry Descriptors from Terrestrial Laser Scanning to Map Chert in Outcrops. *ISPRS J. Photogramm. Remote Sens.* **2014**, *93*, 88–97. [[CrossRef](#)]
24. Humair, F.; Abellan, A.; Carrea, D.; Matasci, B.; Epard, J.-L.; Jaboyedoff, M. Geological Layers Detection and Characterisation Using High Resolution 3D Point Clouds: Example of a Box-Fold in the Swiss Jura Mountains. *Eur. J. Remote Sens.* **2015**, *48*, 541–568. [[CrossRef](#)]
25. Matasci, B.; Carrea, D.; Abellan, A.; Derron, M.-H.; Humair, F.; Jaboyedoff, M.; Metzger, R. Geological Mapping and Fold Modeling Using Terrestrial Laser Scanning Point Clouds: Application to the Dents-Du-Midi Limestone Massif (Switzerland). *Eur. J. Remote Sens.* **2015**, *48*, 569–591. [[CrossRef](#)]
26. Bellian, J.A.; Kerans, C.; Jennette, D.C. Digital Outcrop Models: Applications of Terrestrial Scanning Lidar Technology in Stratigraphic Modeling. *J. Sediment. Res.* **2005**, *75*, 166–176. [[CrossRef](#)]
27. Freski, Y.R.; Hecker, C.; van der Meijde, M.; Setianto, A. The Effects of Alteration Degree, Moisture and Temperature on Laser Return Intensity for Mapping Geothermal Manifestations. *Geothermics* **2021**, *97*, 102250. [[CrossRef](#)]
28. Muraoka, H.; Nasution, A.; Simanjuntak, J.; Dwipa, S.; Takahashi, M.; Takahashi, H. Geology and Geothermal Systems in the Bajawa Volcanic Rift Zone, Flores, Eastern Indonesia. In *Proceedings of the World Geothermal Congress, Antalya, Turkey, 24–29 April 2005*; pp. 1–13.

29. Ministry of Energy and Mineral Resources of the Republic of Indonesia. Potensi Panas Bumi NTT Mencapai 1.266 Mw (Geothermal potential in Nusa Tenggara Timur province reaches 1.266 Mw). Available online: <https://www.esdm.go.id/id/media-center/arsip-berita/potensi-panas-bumi-ntt-mencapai-1266-mw> (accessed on 1 May 2024).
30. Wunderman, R. (Ed.) Global Volcanism Program Report on Inielika (Indonesia). In *Bulletin of the Global Volcanism Network*; Smithsonian Institution: Washington, DC, USA, 2001; Volume 26, p. 9.
31. PT ASI Pudjiastuti Geosurvey LiDAR Data and Aerial Photo Acquisition Report: Bajawa, Flores Island, Indonesia; PT ASI Pudjiastuti Geosurvey: Jakarta, Indonesia, 2018.
32. BMKG of the Republic of Indonesia Meteorological Report of Frans Sales Lega Station, Manggarai, Flores. Available online: <https://dataonline.bmkg.go.id/> (accessed on 15 June 2022).
33. Kashani, A.G.; Olsen, M.J.; Parrish, C.E.; Wilson, N. A Review of LIDAR Radiometric Processing: From Ad Hoc Intensity Correction to Rigorous Radiometric Calibration. *Sensors* **2015**, *15*, 28099–28128. [[CrossRef](#)] [[PubMed](#)]
34. Zhang, W.; Qi, J.; Wan, P.; Wang, H.; Xie, D.; Wang, X.; Yan, G. An Easy-to-Use Airborne LiDAR Data Filtering Method Based on Cloth Simulation. *Remote Sens.* **2016**, *8*, 501. [[CrossRef](#)]
35. Höfle, B.; Pfeifer, N. Correction of Laser Scanning Intensity Data: Data and Model-Driven Approaches. *ISPRS J. Photogramm. Remote Sens.* **2007**, *62*, 415–433. [[CrossRef](#)]
36. Kaasalainen, S.; Hyypä, J.; Litkey, P.; Hyypä, H.; Ahokas, E.; Kukko, A.; Kaartinen, H. Radiometric Calibration of ALS Intensity. *Int. Arch. Photogramm. Remote Sens.* **2007**, *47*, 201–205.
37. Vain, A.; Kaasalainen, S.; Pyysalo, U.; Krooks, A.; Litkey, P. Use of Naturally Available Reference Targets to Calibrate Airborne Laser Scanning Intensity Data. *Sensors* **2009**, *9*, 2780–2796. [[CrossRef](#)] [[PubMed](#)]
38. Yan, W.Y.; Shaker, A. Radiometric Correction and Normalization of Airborne LiDAR Intensity Data for Improving Land-Cover Classification. *IEEE Trans. Geosci. Remote Sens.* **2014**, *52*, 7658–7673. [[CrossRef](#)]
39. El Halim, M.; Daoudi, L.; El Alaoui El Fels, A. How Elemental Composition Influences the Color of Igneous and Sedimentary Rocks: Case of the High Atlas Rocks of Morocco. *Color. Res. Appl.* **2022**, *47*, 475–485. [[CrossRef](#)]
40. Hartzell, P.; Glennie, C.; Biber, K.; Khan, S. Application of Multispectral LiDAR to Automated Virtual Outcrop Geology. *ISPRS J. Photogramm. Remote Sens.* **2014**, *88*, 147–155. [[CrossRef](#)]
41. Jin, J.; De Sloover, L.; Verbeurgt, J.; Stal, C.; Deruyter, G.; Montreuil, A.L.; De Maeyer, P.; De Wulf, A. Measuring Surface Moisture on a Sandy Beach Based on Corrected Intensity Data of a Mobile Terrestrial LiDAR. *Remote Sens.* **2020**, *12*, 209. [[CrossRef](#)]
42. Kaasalainen, S.; Niittymäki, H.; Krooks, A.; Koch, K.; Kaartinen, H.; Vain, A.; Hyypä, H. Effect of Target Moisture on Laser Scanner Intensity. *IEEE Trans. Geosci. Remote Sens.* **2010**, *48*, 2128–2136. [[CrossRef](#)]

**Disclaimer/Publisher’s Note:** The statements, opinions and data contained in all publications are solely those of the individual author(s) and contributor(s) and not of MDPI and/or the editor(s). MDPI and/or the editor(s) disclaim responsibility for any injury to people or property resulting from any ideas, methods, instructions or products referred to in the content.